

Salt-dissolution-induced subsidence in the Dead Sea area detected by applying interferometric techniques to ALOS Palsar Synthetic Aperture Radar images

Damien Closson ^{1*}, Najib Abou Karaki ², Nada Milisavljević ¹,
Frédéric Hallot ¹, Marc Acheroy ¹

¹ Signal and Image Centre, Avenue de la Renaissance 30, Brussels 1000, Belgium

² University of Jordan, Environmental and Applied Geology Department, Amman, Jordan

Abstract

This paper discusses the interpretation of ground motions detected in the dried up Lynch Strait, Dead Sea area, by applying radar interferometric techniques to ALOS Palsar Synthetic Aperture Radar images. Four ALOS scenes spanning from December 15, 2007 to May 17, 2008 have been processed leading to the generation of five interferograms. Three ground deformation zones have been detected. One of them shows surface displacement which could be related to an earthquake (ML 3.1) that took place on April 13, 2008. High rates of subsidence have been measured in the northern Lynch Strait. They suggest that these subsidence phenomena follow the same trend of rapid increase as sinkholes. Additional measurements should be carried out in order to refine this observation.

The comparison between sinkholes' distributions in the Lynch Strait with that of Ghor Al Haditha, six kilometers eastward, supports the idea that the earthquake that hit the southern Dead Sea on April 23, 1979 (M 5.1) reactivated faults and fractures in the Lynch Strait triggering the development of sinkholes and subsidence in the frame of the Dead Sea recession.

© 2010 Lavoisier SAS. All rights reserved

Keywords: Dead Sea, sinkholes, Lynch strait, Alos palsar, interferometry

1. Introduction

1.1. General aspects

The Dead Sea is the saltiest water body in the world with a saline concentration ten times greater than the average sea-water. The current lake level is about -423 m (2010) while it was -395 m in the mid-1960s. The study area corresponds to the dried up Lynch Strait (Fig. 1). Its current size is about 4 km

x 10 km but it is extending northward due to the lowering of the lake level, at an increasing rate, exceeding one meter per year in 2010. The Lynch Strait coincides with a segment of the borderline between Jordan and Israel. It emerged from 1979 to 1982. Its elevation is between -401 m and -402 m.

Before it emerged, the Lynch Strait used to connect the former Dead Sea southern shallow basin (-402 m) to the much deeper northern one (-730 m) (Fig. 1A). Russian topographic maps (Fig. 1B, C) and time series of ERTS (future Landsat)

* Corresponding author.

Tel: +32 2 742 66 66 - Fax: +32 2 742 64 72

Email address: Damien.closson@yahoo.fr

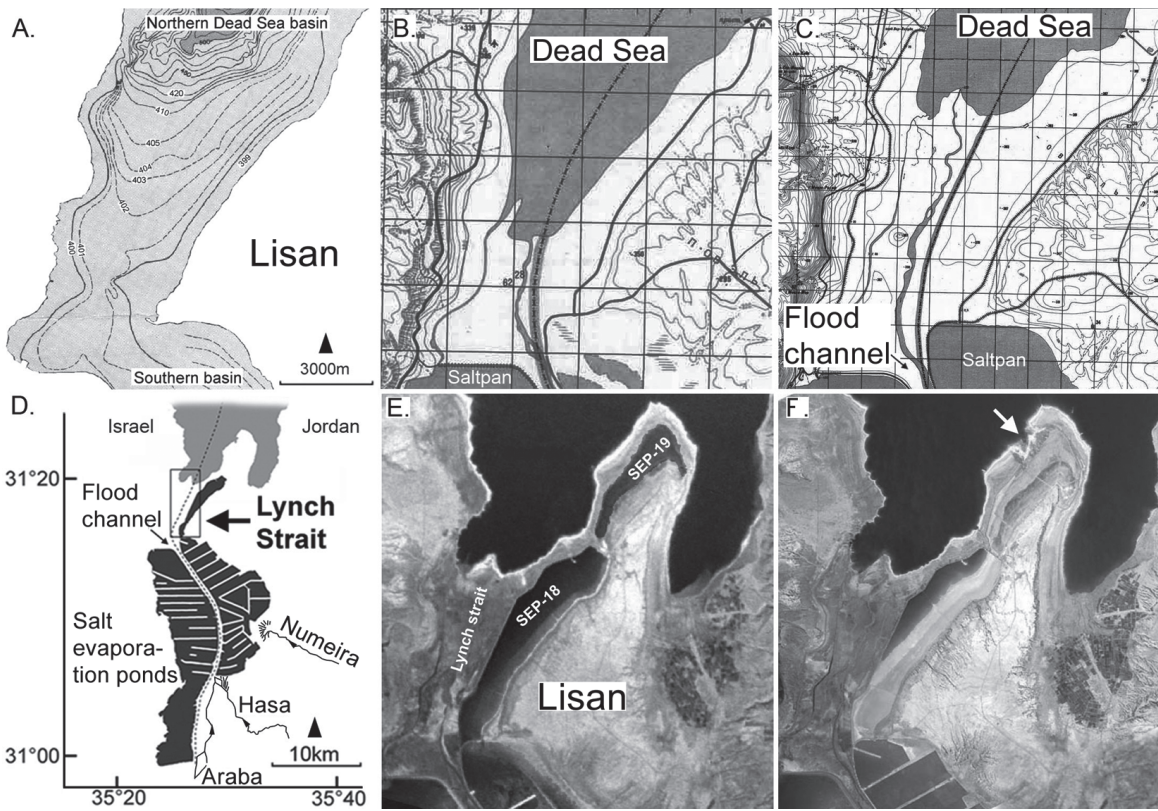


Fig. 1: (A) Bathymetric map [1]; **(B)** Topographic map 8-36-35 at 1:100,000 scale – graticule 2 km, survey 1980 [2]; **(C)** Topographic map 8-36-35-2 at 1:50,000 scale – graticule 1 km, survey 1993. The outlet of the Flood channel is indicated [2]; **(D)** Location map mentioning the Lynch Strait, outlet of the Flood channel, Salt Evaporation ponds, Wadi Numeira, Hasa, and Araba; **(E - F)** Space Shuttle photographs [3] acquired in February 2000 **(E)** and February 2003 **(F)**. SEP-18 and SEP-19 are Salt Evaporation Ponds. White arrow points to the collapsed area of SEP-19 in March 2000.

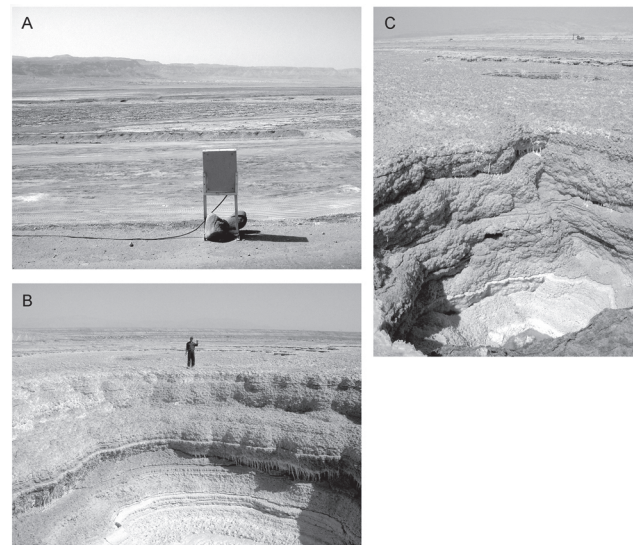
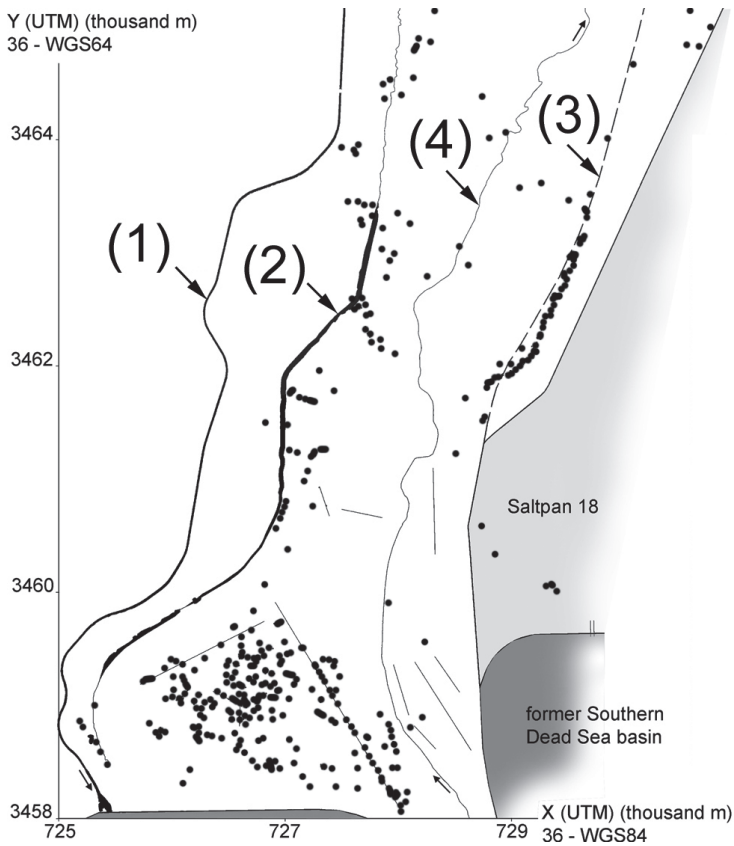


Fig. 2: Central and southern parts of the dried-up Lynch Straits. Sinkholes are represented by small black dots. They appear in clusters or lineaments. Lines have been drawn to indicate the main structural directions at local scale. Major infrastructures are reproduced: **(1)** Dead Sea Works new intake canal; **(2)** old intake canal destroyed by sinkholes; **(3)** Arab Potash Company access road partially destroyed by sinkholes in 1992; **(4)** Wadi Araba constitutes the borderline between Israel and Jordan. **Pictures:** **A** - Lynch Straits observed from saltpan 18. This arid no man's land is characterized by a flat topography; **B** - Decametric sinkholes close to saltpan 18; **C** - metric sinkhole, in the background mechanical diggers are working in order to increase the safety factor of the dike encompassing saltpan 18. Author's pictures acquired on April 28, 2005.

satellite images acquired since 1972 have shown that the Lynch Strait emerged progressively between 1979 and 1982, turning the Lisan Peninsula into a land bridge between the Eastern and the Western shores. The southern basin dried up during the 1970s and was progressively covered by salt evaporation ponds (Fig. 1D – black color) created by the Dead Sea Works and the Arab Potash Company in the 1980s (Fig. 1B, 1C).

To avoid damage in the dikes of the salt pans during flash floods, a 550 m width earth channel has been built on the border between Israel and Jordan (Fig. 1C, D “flood channel”). This canal evacuates the waters of Wadi Hasa, Wadi Numeira, and Wadi Araba, which use to flow into the southern basin, to the northern basin (Fig. 1D). The water flow in this canal has progressively incised the deposits of the Lynch Strait, creating abandoned meanders and terraces (Fig. 1C). As the base level lowers rapidly, year after year the stream becomes more entrenched in the soft deposits. The steep river banks are affected by undermining and sliding and the transported sediments feed a delta that continuously progrades seaward.

In the 1990s, the Arab Potash Company extended its industrial plant over part of the Lynch Strait and the neighboring Lisan peninsula. As a result, two major production units (Fig. 1E, SEP-18 and SEP-19) were built over the recently emerged lands. The 38 million USD salt evaporation pond 19 (Fig. 1E, SEP-19) was destroyed due to sinkholes and subsidence during the first filling in March 2000. The white arrow of Figure 1F indicates the area eroded by the rapid discharge of 55 million cubic meters of Dead Sea brine in less than one hour. A section 1650 m long of the dike surrounding the pond disappeared completely. Saltpan 18 (32 million USD) is suffering from subsidence and sinkhole damages since its construction in the mid-1990s. It was repaired from 2001 to 2006 (16 million USD) to increase the safety factor of the dike. The width of the embankment was even tripled in the most suffering areas.

1.2. Problem statement

On average, the annual rainfall is less than 70 mm in the southern Dead Sea area. In such arid conditions salt deposits are widespread and resist erosion by dissolution for a relatively long period. The salt deposits are so frequent in the Dead Sea area that the shore areas can be considered as a salt karst system. When a flash flood event occurs in the dried up Lynch Strait, the sudden interaction between salty sediments and unsaturated water causes significant dissolution. Under these conditions the landscape may change very quickly. As an example, a major flood occurred over a 24-hour period on March 22, 1991, which was caused by a short and intense rainfall event. Runoff from Wadi Hasa and Wadi Numeira discharged into the flood channel (Fig. 1D). The lake level rose from -407.701 m on February 27, 1991 to -407.512m after the flood (Arab Potash Company’s gauge station), contrary to the steady decline trend in the Dead Sea level. On the basis of this rise and descriptions on the distribution of rainfall, it was estimated that the flood volume that flowed through the

flood channel was of the order of 100 million cubic meters over a 24-hour period [4].

This storm and flood event triggered hundreds of collapse sinkholes with vertical walls and diameters of 5-20 m (Fig. 2). On the Jordanian side, the sinkholes define a remarkable kilometeric lineament with a NE-SW direction consistent with the main structural trend of the western boundary fault system of the Dead Sea pull-apart basin (Fig. 2 - coordinates 729, 3462). A practical consequence of this event was the reshaping of the future saltpan 18 since an access road, which was planned to turn into a dike, was destroyed by sinkholes (Fig. 2 – coordinates 729 – 3464).

Aerial photographs reveal that sinkholes already existed in 1982 (e.g. [5]). This is not surprising because 1981 was also characterized by a rainy winter; the Dead Sea level rose about 20 cm in February 1981.

From a geological point of view, the Lynch Strait is situated over the limit between the Sinai sub-plate and the Arabian Plate. It is a kilometeric graben filled with lacustrine-fluvial sediments within the Dead Sea pull-apart basin, a key structure of the 1000 km long Jordan - Dead Sea transform fault zone connecting the Red Sea rift to the Taurus Mountains. The recent activity of the faults bounding the Lynch Strait (during the late Dead Sea Depression deformation) is indicated by prominent bathymetric relief, control of young sedimentation, association with linear arrays of collapse sinkholes, and current seismicity produced by left lateral strike-slip with a normal component [6].

The Lynch fault zone consists of at least two main faults that control a linear array of sinkholes and ground depressions. The importance of the Lynch fault as a deep-penetrating fault is demonstrated by seismic refraction profiles about 100 km in length that suggest a major southward down-faulting where the trace of the Lynch fault is crossed [6].

1.3. Goal of this work

This paper discusses the interpretation of ground deformation detected in the recently dried up Lynch Strait by applying radar interferometry technique to ALOS Palsar Synthetic Aperture Radar (SAR) images. Four ALOS scenes spanning from November 15, 2007 to May 17, 2008 have been processed, resulting in the generation of five interferograms. The detected movements are interpreted in the light of their geological context.

2. Material and method

2.1. Material

The four ALOS Palsar images processed in this work belong to track 251 – frame 2990 (acquisitions of May 17, 2008; April 1, 2008; February 15, 2008; November 15, 2007). The scenes (70 km x 70 km – descending mode) cover a wide part of the Negev desert and the southern Dead Sea area.

Field surveys were carried out in May, 2008 in the frame of the monitoring of ground deformations over the Lisan peninsula and the Lynch Strait [e.g. 7]. A Global Positioning System (GPS) has been used to record evidence of the ground displacements and the observation points were incorporated in a Geographical Information System (GIS).

2.2. Method

2.2.1. Radar Interferometry Techniques

Radar interferometry techniques have been applied to investigate ground motions occurred from November 15, 2007 to May 17, 2008. Pixels in a radar image are complex numbers where the argument (the phase of the emitted/received signal) represents a measure of the distance between the antenna and the ground. An interferogram is formed when two radar images are co-registered and the phase difference between corresponding pixels is computed. The phase difference for any point of the ground takes a value ranging from 0 to 360 degrees. Each complete 360 degree cycle corresponds to a unique surface (one “fringe”) over an interferogram characterized by a specific elevation interval. The “altitude of ambiguity” represents this interval and is a function of the radar wavelength, satellite altitude, incidence angle, and baseline.

If two radar images are acquired simultaneously from slightly different locations (Fig. 3), the interferometric phase is sensitive to the surface topography. When two images are acquired at two different moments, the interferometric phase is sensitive to the surface topography and the displacements of the ground parallel to the radar line of sight occurred during the acquisition time interval.

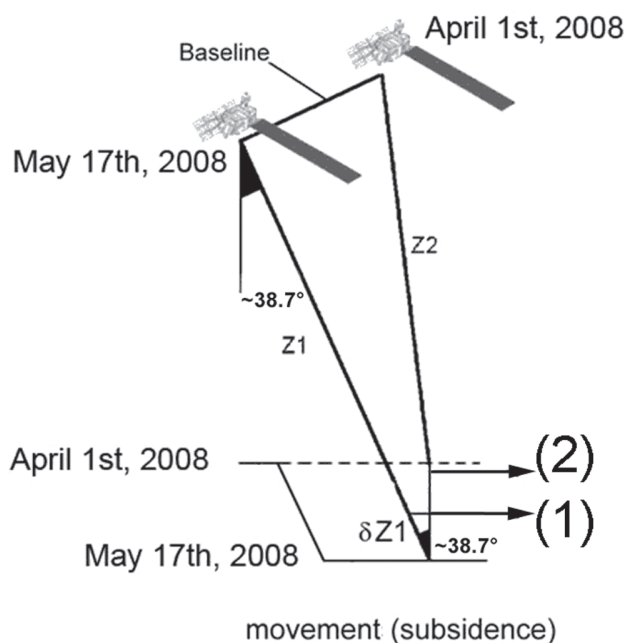


Fig. 3: interferometric synthetic aperture radar geometry (ALOS perspective) in the case of subsidence detected in the line of sight (1) and projected in the vertical plane (2).

While the “altitude of ambiguity” decreases when the distance between the two orbits increases, the sensitivity to the ground displacements is independent of the satellite configuration. For space-borne imaging radar systems, sensitivity to the ground displacements is generally a few thousand times greater than the sensitivity to topography, allowing the detection displacements of a few millimeters [e.g. 8-9].

The main limitations of the radar interferometry techniques are related to the lack of coherence between two acquisitions, atmospheric refraction and precise targeting [e.g. 10]. In this work, the interferograms were computed with the “Radar Mapping Suite” of Erdas Imagine 2010 and the module Sarscape of Envi.

2.2.2. Deformation measurements

Ground displacements are measured in the line of sight of the radar antenna as shown on Figure 3. They can be decomposed into vertical and horizontal motions. In this article, only vertical motions will be considered. Figure 3 is a simplified representation of the geometry of acquisition of two images with a subsiding target. The interferometric baseline of the pair April 1 - May 17, 2008 is very short (17 m). In this case the topographic component is negligible and the resulting interferogram bears only a differential phase component related to the time interval between the two acquisitions (minimum ALOS revisit time is 46 days).

During the processing, the April 1, 2008 (“slave”) scene was co-registered over the May 17, 2008 image (“master”). The April 1st image is considered as a fixed reference. The displacements recorded by the May 17, 2008 image are considered in the vertical direction.

The measure of the phase can be expressed as:

$$\Delta\phi = \phi(\text{April 1, 2008}) - \phi(\text{May 17, 2008})$$

$$\Delta\phi = 2 * (Z2 - Z1) / \lambda * 2\pi \text{ rad}$$

$$\Delta\phi = (4\pi/\lambda) * (Z2 - Z1 - \delta Z1)$$

$$\Delta\phi = (4\pi/\lambda) * (Z2 - Z1) - (4\pi/\lambda) * \delta Z1$$

In the case of estimation April 1, 2008 to May 17, 2008, the measure is negative: $-(4\pi/\lambda) * \delta Z1$. This means that when one goes from point A to point B over the interferogram (Fig. 4) and the phase increases (from black to white), the movement is oriented toward the satellite. Or, point A goes away from the satellite in relation to B.

Φ increase: $-(4\pi/\lambda) * \delta Z1 > 0$ then $\delta Z1$ is negative

→ comes closer to the satellite

Φ decrease: $-(4\pi/\lambda) * \delta Z1 < 0$ then $\delta Z1$ is positive

→ moves away from the satellite

In the case of estimation May 17, 2008 to April 1, 2008, the measure is positive: $+(4\pi/\lambda) * \delta Z2$

Φ increase: $+(4\pi/\lambda) * \delta Z2 < 0$ then $\delta Z2$ is positive

→ moves away from the satellite

Φ decrease: $+(4\pi/\lambda) * \delta Z2 > 0$ then $\delta Z2$ is negative

→ comes closer to the satellite

Five interferograms have been unwrapped and multiplied by $(0.118 \text{ m}/2\pi) * \cos \alpha$ ($\alpha \sim 38.7^\circ$) in order to measure motions in the line of sight, vertically and horizontally.

2.2.3. Error estimation in the measurements

Phase error is given by the coherence value [0 to 1] evaluated for each pixel by the relation:

$$\text{Phase error} \geq [1 / (2n) * \frac{1}{2}] * [1 - (\text{coherence})^2 / (\text{coherence})^2]$$

For example, if one chooses a coherence value equal to 0.7 in order to have 10° of phase error (i.e. 1/36 of circle), for the targets with a coherence value ≥ 0.7 the error is:

- ≤ to [altitude of ambiguity / 36] for elevation data,
- ≤ [ALOS wavelength / 36] for ground motions.

2.2.4. ALOS and ERS space-borne sensors over the Dead Sea

Radar interferometry techniques have been successfully used for years to study ground deformation in the Dead Sea area. Up to now, the main results were obtained processing ERS-1 and ERS-2 satellite data (e.g. [11-17]). While the ERS sensors were characterized by C-band and VV polarization, ALOS Palsar uses L-band, and in this work HH polarization was selected. Table 1 highlights some characteristics, advantages and drawbacks in the use of ERS or ALOS space-borne sensors [based on 18-19].

Table 1: Some elements of comparison between imaging radars onboard ERS and ALOS satellites.

	ERS (C band)	ALOS (L band)
Altitude of the satellite	~789 km	~700 km
Frequency band	5.3 GHz	1.27 GHz
Wavelength	5.6 cm	23.6 cm
Polarization	VV	HH/HV or VV/VH
Incidence angle	~23.2°	~38.7°
Maximum perpendicular baseline	1100 m	15380 m
Resolution (range)	~24.5 m	~8.6 m
Resolution (azimuth)	~5 m	~5 m
Swath	~100 km	~70 km
Repeat cycle	35 days	46 days
phase noise (*)	2.1 mm	3.3 mm
fringe rate	4	1
Coherence	less	better
Tropospheric effects	Identical	Identical
Ionospheric effects	better	~17 times greater at L-band than C-band
Phase gradients / Greater deformation	less	better
Measurement accuracy	better	Less (~1.6 times)

(*) i.e., line of sight (LOS) precision of over the 100 m to 5000 m wavelength band

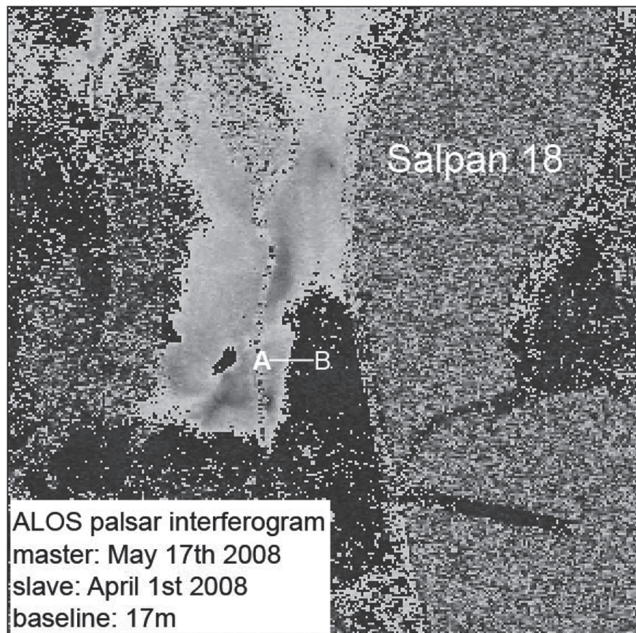


Fig. 4: Phase (Φ) evolution along profile A-B (southern Lynch Strait area) over the interferogram generated from ALOS images acquired on April 1, 2008 and May 17, 2008.

The expression “HH polarization” means that radio waves were transmitted by the antenna such that the radiation was horizontally polarized, and then that the antenna only received horizontally polarized radiation. HH polarization is the preferred polarization in the study of soil moisture.

2.2.5. Characteristics of ALOS images pairs used in this study

An interferogram created from two images acquired at two different times from slightly different locations displays “fringes” sensitive to the topography and the displacements (existing, detectable) occurred over the time interval. If one focuses only on the ground movements, the “topographic fringes” have to be retrieved. However, in two cases this subtraction is not mandatory to clearly identify the displacement “fringes”.

The first case is when a pair of images has been acquired from nearly the same position. In this work, one interferogram has been generated from a pair of images (April 1, 2008 - May 17, 2008) with a perpendicular baseline of 17 m leading to an “altitude of ambiguity” of 2705 m. The elevation over the ALOS scene ranges between -422 m to 971 m. Taking this into account, if one can see concentrated fringes over such an interferogram, then a ground displacement is suspected, and more so if the fringes are located in flat areas like the Lynch Strait or the southern Dead Sea shore.

The second case concerns two other pairs (April 1, 2008 - February 15, 2008 - November 15, 2007) with an “altitude of ambiguity” that is wide with respect to the slope gradient

Table 2: Main characteristics of the interferometric pairs displayed on Figure 5.

Interferogram	Acquisition dates	ΔT	Perpendicular baseline	Altitude of ambiguity
B	01Apr08 - 17May08	46 days	17 m	2705 m
C	15Feb08 - 01Apr08	46 days	555 m	83 m
D	15Nov07 - 15Feb08	92 days	477 m	96 m
E	15Feb08 - 17May08	92 days	572 m	112 m
F	15Nov07 - 17May08	184 days	1049 m	61 m

Table 3: Zone A, amplitude of the ground displacements evaluated from the profiles (Figures 6 and 7).

	15Nov07-15Feb08	15Feb08-01Apr08	01Apr08-17May08	15Feb08-17May08	15Nov07-17May08
Northern	4 cm	8 cm	4 cm	6 cm	15 cm
Central	2.5 cm	5 cm	8 cm	10 cm	12 cm
South	1.5 cm	4 cm	9 cm	10 cm	12 cm

of the studied area. In that case, the “topographic fringes” do not impact significantly over the “displacement fringes”. For example, in the Lynch Strait the slope gradient ($0^\circ - 1^\circ$) is very small as inferred from the distance between contours in Figure 1A, 1B, 1C, and field photographs Figure 2A, 2B, 2C. In this work, four interferograms with an “altitude of ambiguity” of 61 m, 83 m, 96 m, and 112 m have been computed. Hence, as the elevation of the Lynch Strait ranges from -403m (sides) to -422m (Dead Sea shore in 2009), in such interferograms around 1/4 of a topographic fringe covers the area of interest. So, again, if one phase jump is observed, then ground displacement is suspected.

Finally, one has to recall some characteristics of the Lynch Strait that make it very attractive for a successful study based on radar interferometry:

- the local slope gradient is close to zero. Steep river banks are found along the Wadi Araba;
- coherence losses due to human activities are nonexistent;
- the climate is extremely hot and dry and thus the area is devoid of vegetation. Only moisture, too rapid subsidence for the Palsar L-band sensor and collapses are able to decorrelate the signal.

3. Results

3.1. Geocoded unwrapped differential interferograms

Figure 5 shows an overview of the Lynch Strait’s ground motion areas mapped between November 15, 2007 and May 17, 2008 (184 days). Inset A is an ALOS AVNIR-2 RGB composite acquired on April 19, 2009. It shows the landscape in the visible wavelengths about one year after the latest radar acquisition. Three white boxes delineate zones A, B and C affected by ground subsidence. The landscape of zone A has been photographed from the dike of saltpan 18 (Fig. 2A), it is a very flat area crossed by Wadi Araba. Zone B corresponds to the delta of Wadi Araba. Zone C shows the brine intake station of the Arab Potash Company. It is at the periphery

of the Lynch Strait and has already been recognized as a subsidence area over at least one differential interferogram covering a period from June 11, 1992 to August 5, 1993 [7]. Sinkholes have affected this site for more than 10 years [19]. Therefore, it will not be analyzed in this article.

Insets B to F are five geocoded unwrapped interferograms (UTM 36, WGS 84). Table 2 provides the main characteristics of the interferometric pairs. Water surfaces have been masked to hide strongly decorrelated zones and to facilitate the interpretation.

Interferograms B, C and D constitute a time sequence while interferograms E and F synthesize the ground displacements of B and C (92 days) and B, C and D (184 days). The various combinations indicate the lack of artifacts.

Zones A, B and C appear in all interferometric combinations (B to F) with extend and subsidence rates. Interferogram F displays the three zones with more contrasts because it sums the information of B, C and D or D and E.

Due to the short perpendicular baseline (17 m – Table 2), interferogram B does not present any topographic phase residues. The altitude of ambiguity equal to 2705 m is greater than the elevation range of the area covered by the scene (from +971 m to -422 m). Therefore, in this case, any phase jump can be interpreted as a potential indicator of ground motion, especially if the fringes are located in zones such as the southern Dead Sea shores, where subsidence has been well known for years.

Regarding the overall coherence, as expected, the values are generally high over the Lynch Strait. The most important low values are located in the southern and central parts, especially over the shallow swamps situated between coordinates 726 – 727 and 3459 – 3460 (Fig. 2).

3.2. Spatial evolution of the deformation zones

The spatial and temporal evolution of the deformation zones (from the stable area to the most affected) can be described through series of profiles (Figures 6 - 8). On

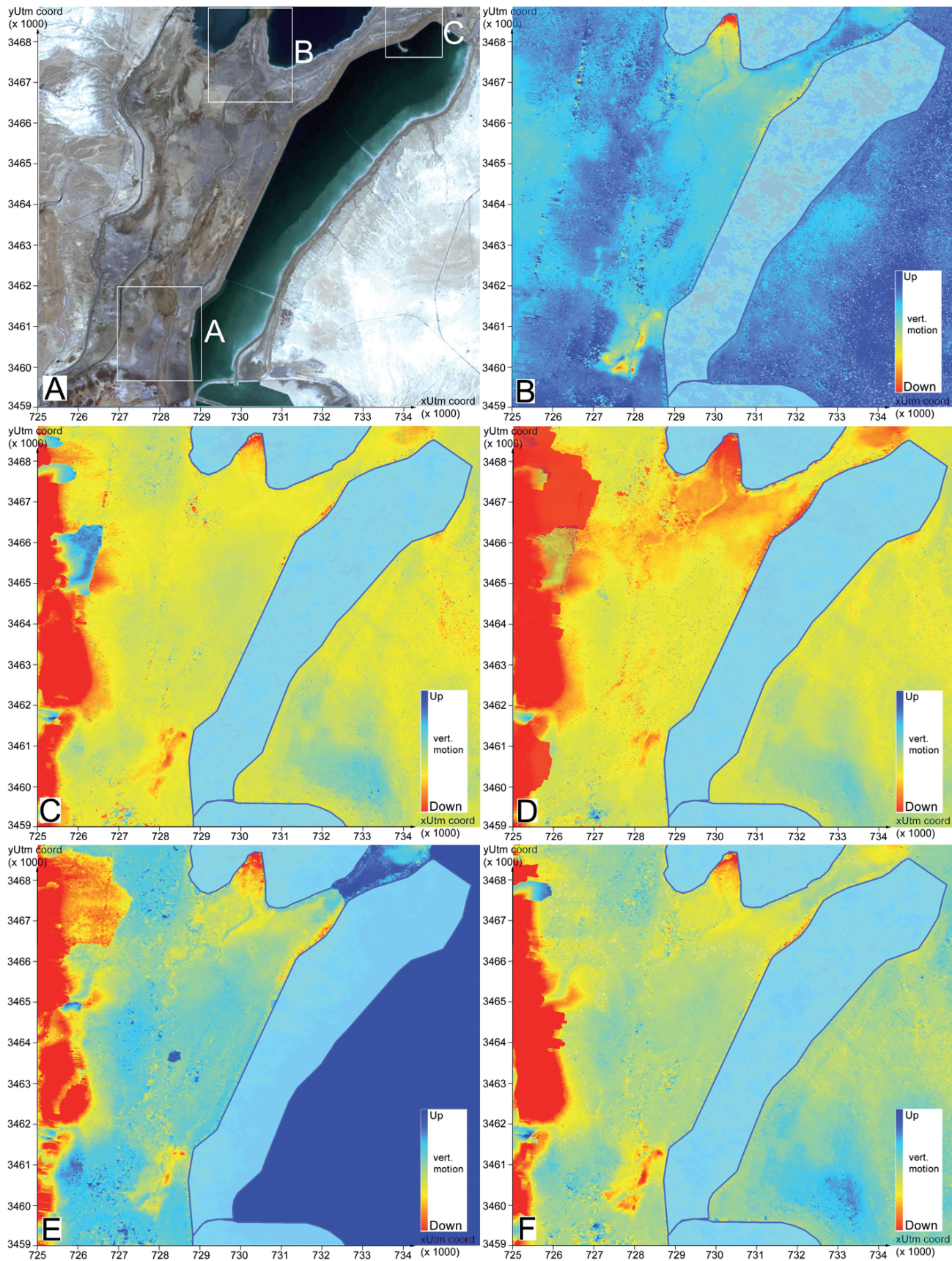


Fig. 5: Differential interferograms. Table 2 summarizes the main characteristics. Highly decorrelated surfaces corresponding to water have been masked (saltpan, Dead Sea).

Table 4: Zone B, amplitude of the ground displacements evaluated from one profile (Fig. 8).

	15Nov07-15Feb08	15Feb08-1Apr08	1Apr08-17May08	15Feb08-17May08	15Nov07-17May08
N-S profile	11 cm	8 cm	6 cm	20 cm	14 cm

Table 5: Comparison between subsidence rates of the Wadi Araba delta acquired with interferometric pairs characterized by small perpendicular baselines (topography “free”).

Acquisition dates	Sensors	ΔT	Perpendicular baseline	Altitude of ambiguity
30Jul95 – 11Dec95	ERS - AMI	104	6 m	1474 m
Subsidence 30 mm \Rightarrow Rate of subsidence: 105 mm/year				
11Dec95 – 09Feb97	ERS - AMI	456	2 m	4422 m
Subsidence 80 mm \Rightarrow Rate of subsidence: 64 mm/year				
01Apr08 – 17May08	ALOS - PALSAR	46	17 m	2705 m
Subsidence 60 mm \Rightarrow Rate of subsidence: 476 mm/year				

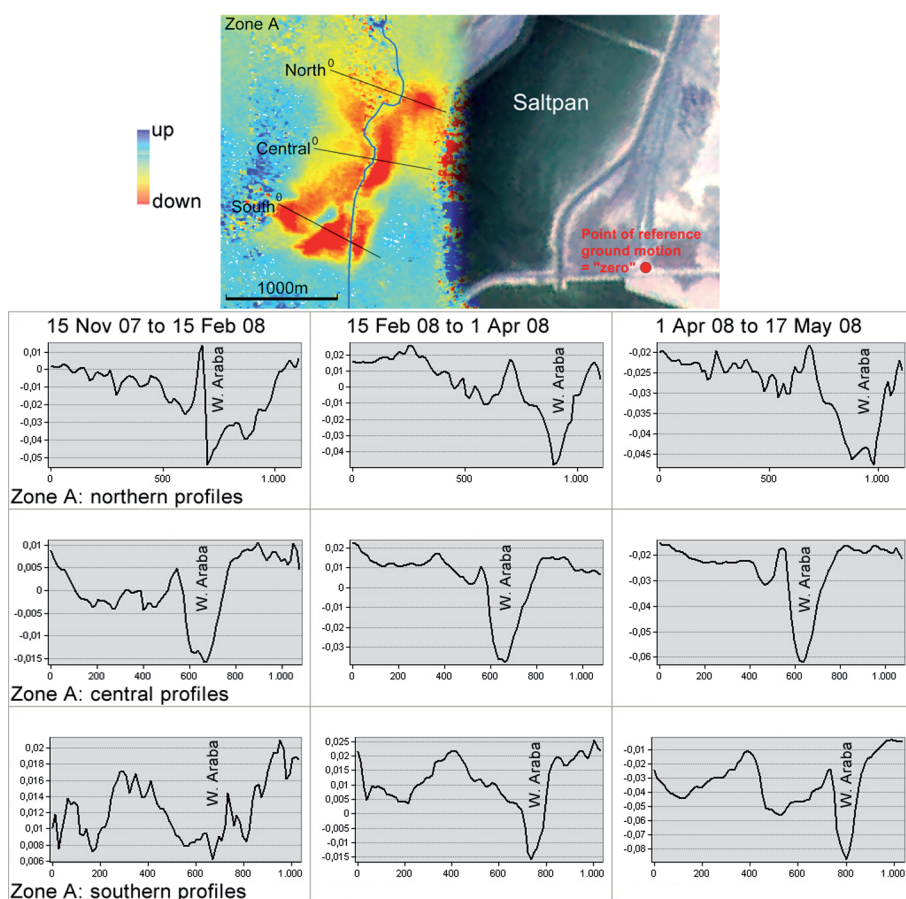


Fig. 6: Zone A - profiles showing the extent and evolution of measured deformation along three selected transects for the period corresponding to interferograms B, C and D (Fig. 5)

Figure 6, the upper inset shows the trace of three profiles (North, Central, and South) crossing zone A over the differential interferogram April 1, 2008 - May 17, 2008. One “point of reference” is indicated. In this study, it has been arbitrarily defined as a “stable” point (ground motion = zero). In the ideal case, it corresponds to a point monitored with a GPS in order to get the value of the vertical and horizontal components of displacement. During the interferometric processing, the phase value of this point

is subtracted from each unwrapped phase value to obtain the “absolute” displacement components for the output map images. Hence, incorrect setting of the zero reference point would result in a constant artificial displacement in the deformation map.

3.3. Ground motions

3.3.1. Zone A

Table 3 synthesizes the amplitude of the vertical motions (subsidence) in zone A recorded through three profiles (see Figure 6) over five interferograms.

From November 15, 2007 to February 15, 2008 the northern part was the most active. From February 15, 2008 to April 1, 2008 the subsidence increases in the three profiles and the values recorded double those of the previous observation period. Finally, from April 1, 2008 to May 17, 2008 the trends observed at the beginning reversed; the southern sector was the most active, followed by the central part. The subsidence decreases in the northern segment while it increases in the central and southern parts.

3.3.2. Zone B

Table 4 shows the subsidence values recorded for the delta of Wadi Araba.

When comparing subsidence values of Table 5, one has to keep in mind that the position of the delta in the mid-1990s was about 1700 m SSW from the location in 2008. Consequently, the location of the profiles differ. The Dead Sea elevation was about -400 m against -422 m at present

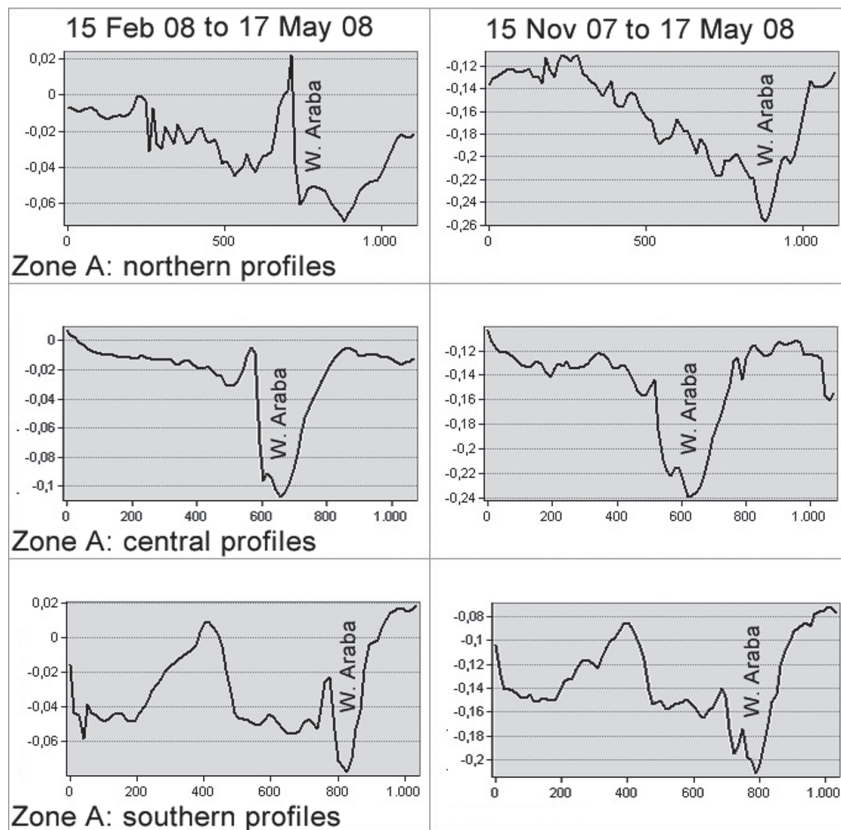


Fig. 7: Zone A - profiles showing the extent and evolution of measured deformation along three selected profiles for the period corresponding to interferograms E and F (see Figure 5)

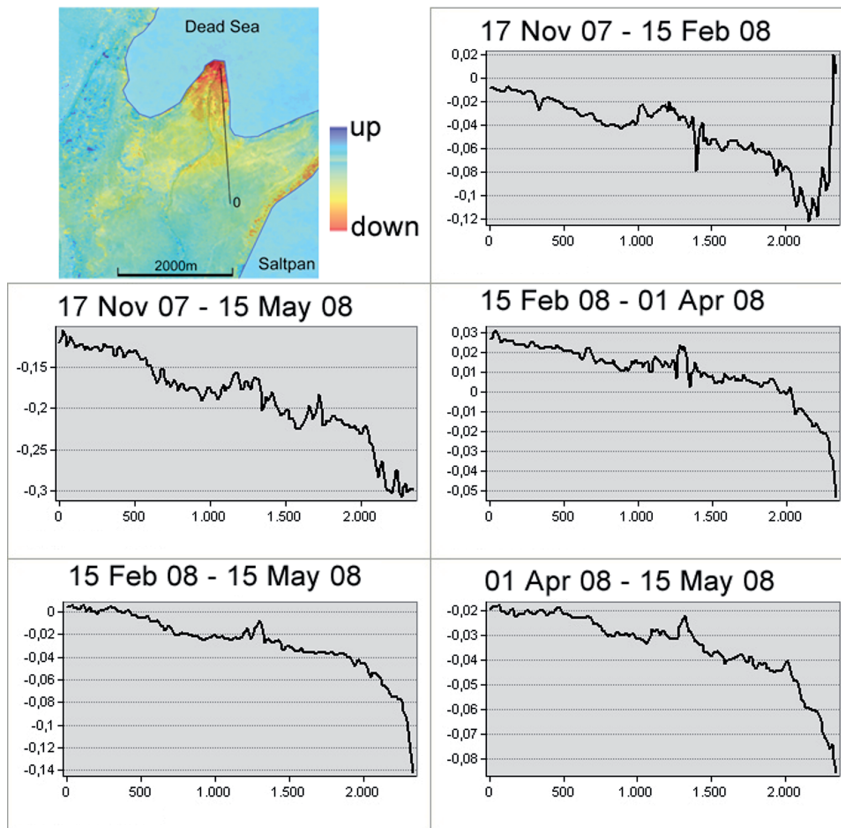


Fig. 8: Zone B - profiles showing the extent and evolution of measured deformation along one selected profile for the period corresponding to interferograms B, C, D, E, and F (Fig. 5)

and the lowering rate was about 80 cm per year in comparison with 120 cm per year at the present time.

3.4. Lynch Strait's global subsidence

Figure 9 focuses on a wide fringe encompassing the Lynch Strait over the interferogram April 1, 2008 - May 17, 2008. As previously mentioned, the altitude of ambiguity of this pair is by far greater than the elevation amplitude in the area covered by the entire ALOS pascars scene (70 km – elevation ranges from 971 m to -422 m). Therefore, the phase jump underlined with red denotes that a major event happened in this area between the two acquisitions. One can also deduce that the loss of coherence caused by water in saltpan 18 and the Dead Sea masks an important part of this fringe. The angular variations of direction well visible in the southern part (corresponding to zone A – see also Figure 4) suggest that a seismic event could be at the origin of the phenomena.

4. Discussion

4.1. Major subsidence event during the monitoring period

The interferogram displayed on Figure 9 raises question about an event able to produce one fringe jump over the whole Lynch Strait between April 1, 2008 and May 17, 2008. A possible interpretation can be found in the earthquake records of the European-Mediterranean Seismological Centre. Indeed, two earthquakes hit the southern Dead Sea between the two acquisitions. The first event occurred on April 13, 2008 at 08:17:43.4 UTC. It had a magnitude ML 3.1, the epicentral location was 31.29 N - 35.44 E, and the focal depth 16 km. Its epicenter is located inside saltpan 18, i.e. precisely inside the whole subsiding area. Seven minutes later it was followed by another event (08:24:18.3 UTC); Mw 2.3, location 31.30 N - 35.55 E, depth 10 km, in the Ghor Al Haditha area, Jordan, about six kilometers eastward.

Field observations were carried out on May 19th, 2008 (five weeks after the ML 3.1 earthquake) all along the dike of saltpan 18. Sinkholes and fractures were photographed and recorded with a GPS.

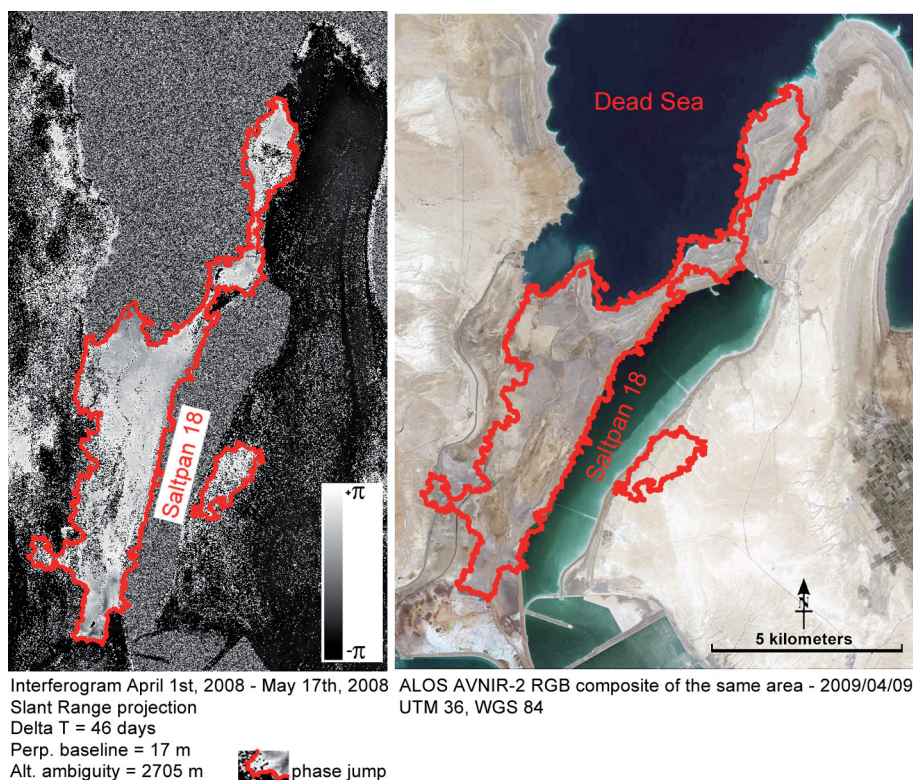


Fig. 9: Wide fringe encompassing the Lynch Strait over the interferogram April 1, 2008 - May 17, 2008

Sinkhole alignments and ground motion fringes complement the available information related to the structural setting. The intersected lineaments at coordinates 729-3462 reflect the N 24 E and N 66 E structural directions (Fig. 2). On the interferograms

was established by Arieh *et al* [22]. It shows that the seismogenic fault corresponds to a NNE trending, left-lateral fault with normal component (Fig. 11). This focal mechanism can be considered as representative of the earthquakes generated on faults with the general direction of the Jordan - Dead Sea Transform fault system in the east coast of the Dead Sea area.

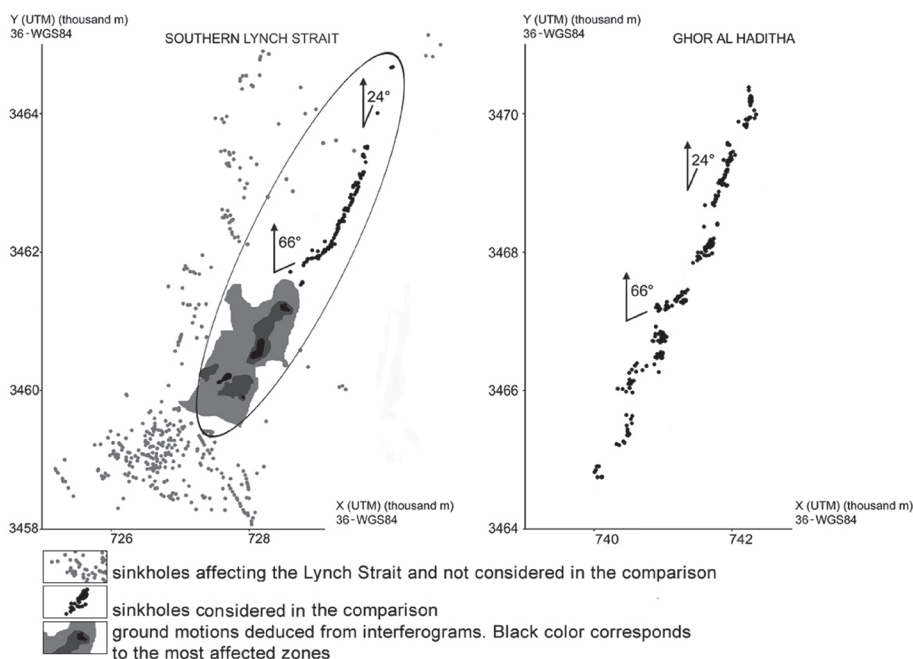


Fig. 10: Comparison at the same scale of the distribution of sinkholes in the Lynch strait area and in Ghor Al Haditha. The directions (24° and 66°) of sinkhole alignments are indicated. The ellipse points the area having recorded the most important deformation during the monitoring with ALOS Palsar images. See also Figure 11 for the relative location of the two lineaments.

displayed on Figure 5 (zone “A”) similar orientations are observed in many places. The agreement between the directions of some fringe segments and the ones displayed by the sinkhole alignments supports the idea of a structure about four kilometers in length and half a kilometer in width. Its zigzagging shape is characteristic of deformations controlled by strike-slip faults.

It is interesting to note the similarity between the orientation of the fault-controlled tectonic pattern displayed in the southern Lynch Strait and that of an alignment of sinkholes six kilometers long in Ghor Al Haditha few kilometers eastward (Fig. 10), at the place where the second epicenter is located. Recently [21] it has been shown that the direction of the sinkhole alignment in Ghor Al Haditha is consistent with the fault plane deduced from the focal mechanism of the most important instrumental earthquake located in the Lisan area in the past decades: i.e. the Mb =5.1 (N 20 E ± 5 deg) earthquake of April 23, 1979. The focal mechanism

The lineament of sinkholes in Ghor Al Haditha is the longest alignment of collapses documented along the Dead Sea shore. It gathers about 90% of the sinkholes affecting the Eastern coast. With its four kilometers in length, the belt of sinkholes and subsidence depressions affecting the Lynch Strait is the second one in importance in the whole Dead Sea area (Fig. 10 – ellipse). Therefore this lineament, as the one of Ghor Al Haditha is relevant for understanding of the causal factors involved in the origin of the sinkholes along the Dead Sea shore.

Figure 10 compares the distribution of sinkholes in the Lynch Strait and in Ghor Al Haditha. At first glance, the number of sinkholes affecting the Lynch Strait is higher

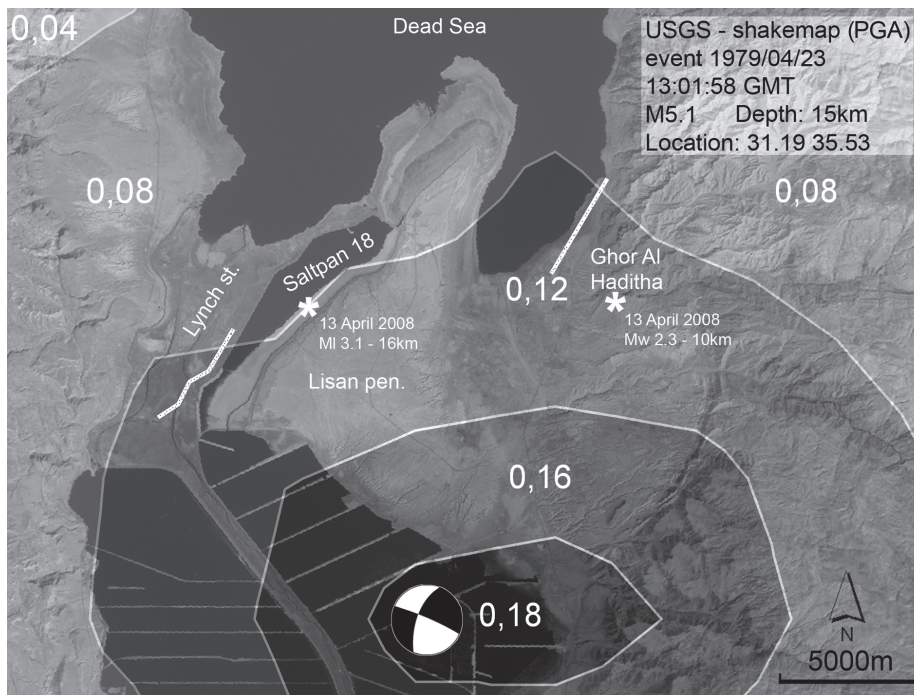


Fig. 11: shake map of the ML 5.1 earthquake, April 23, 1979. Peak Ground Acceleration contours have been computed by the U.S. Geological Survey [27]. The focal mechanism had been established by Arieh *et al* [22]. The locations of the epicenter of the two earthquakes of 13 April 2008 have been provided by the European-Mediterranean Seismological Centre. In terms of accuracy, given the relatively good coverage of the region by seismological stations the accuracy is generally believed to be better than \pm few km for the epicenter coordinates and sometimes much worse for the depth.

than the one of Ghor Al Haditha. However, the difference is probably not so important because Ghor Al Haditha is a farming area and many sinkholes have been filled to avoid incidents. The missing information is however confined inside the damaged zone [21]. The comparison at the same scale clearly shows that the sinkholes follow very similar trends in both areas. Another remarkable similarity is the zig-zag pattern along the lineaments.

Hence, based on these two main geometric characteristics, one can postulate that the causal mechanism of the sinkholes and subsidence depressions inside the ellipse could be the same as the one that produced the lineament of Ghor Al Haditha: i.e. the earthquake of April 23, 1979.

However, in order to understand the sinkhole dynamics, one has to keep in mind two major elements. The first one is that the earthquakes that have hit the Southern Dead Sea area since the lake level began dropping are not the sources of the subsurface cavities revealed by the alignments of sinkholes. Their energy was too low to create ruptures at the ground surface. They could possibly reactivate some segments but not create them. Secondly, the lack of accuracy in the hypocenter locations impedes the establish-

ment of a robust correlation between karst development and seismic events. A precise location of the epicenter is needed to show a correlation between the alignments of sinkholes and the seismic activity.

However, this should not prevent further investigation into the relation between seismicity and sinkholes based on the available material. The U.S. Geological Survey provides Peak Ground Acceleration (PGA) data about the earthquake of April 23, 1979 located in the southern Dead Sea basin (Lat: 31.1910, Lon: 35.5290, Depth: 15 km). Figure 11 depicts PGA values over a Landsat image acquired in 2002, together with the sinkhole alignments of the Lynch Strait and of Ghor Al Haditha, and the two epicenters of the April 13, 2008 events. The area affected by the strongest ground motion (PGA = 0,18 and PGA = 0,16) is outside the zones under the influence of the Dead Sea lowering. The most remarkable feature in this zone is the salt collapse of Birkat el Haj described in [7].

The area with by PGA = 0,12 encompasses new emerged lands and the sinkholes lineaments (white color) of the Lynch Strait and of Ghor al Haditha. It is also the area where the two epicenters are located.

Based on the global distribution of the sinkholes along the Dead Sea shore [22], more than 80% of the recorded sinkholes along the Dead Sea coast occur in the area with PGA of 0,08 and 0,12. This observation supports the idea that the Mb = 5.1 earthquake of April 23, 1979 is one of the main causal factors that have controlled the spatial distribution

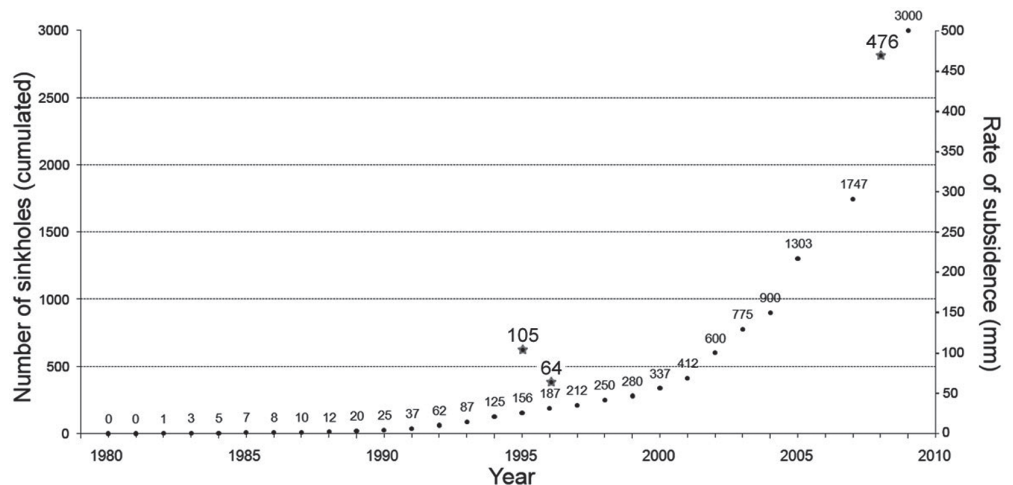


Fig. 12: Cumulative number of sinkholes along the Western shore of the Dead Sea from 1980 to 2009 (black dots). Asterisks indicate the rates of subsidence measured by radar interferometry (Table 2).

of sinkholes in this area, which was already mature enough for such phenomena due to hydrogeological factors induced by human activities during the previous few decades. The important causal factors include a specific salt layer in which dissolutional cavities develop, the presence of discontinuities (faults, fissures), and the shifting of the Dead Sea water / fresh water interface towards the lake. [e.g. 24-26].

The comparison between zone "A" (Fig. 5) with the sinkholes alignment of Ghor Al Haditha supports the idea that the earthquake that hit the southern Dead Sea in April 1979 reactivated fractures in the Lynch Strait along with sinkholes and subsidence have subsequently formed in the frame of the Dead Sea recession.

Note that the earthquake of April 1979 occurred a few years before the very first occurrence of sinkholes in the Dead Sea shore (Fig. 12). This observation suggests that the presence of a shallow salt layer, and the seaward displacement of the fresh/sea water [e.g. 24-26], and faults [17] were not sufficient to trigger the massive appearance of sinkholes and subsidence. Indeed, the level of the Dead Sea started lowering in the sixties, but the first sinkholes appeared only 15 to 20 years later. The only seismic event in this area is the earthquake of 1979. This fact suggests that it reactivated a large number of blind, concealed faults in the southern Dead Sea, creating favorable conditions for the development of sinkholes, e.g. by increasing permeability and ground water circulation and reducing the mechanical strength of sediments overlying the salt layers. This hypothesis is supported by the fact that the majority of collapses are located in the southern part [23]; from Ein Gedi to the Lynch Strait in Israel, and from the Lynch Strait to Ghor Al Haditha in Jordan. PGA data related to the 1979 earthquake support this idea.

4.2. Subsidence of the Wadi Araba delta

Zone "B" of Figure 5, includes a subsidence area affecting the Wadi Araba delta. In such an environment, subsidence is expected due to the continuous supply of poorly consolidated deposits. Previous studies have shown a high subsidence in this area in the mid-1990s. Baer *et al.* [14] measured subsidence rates of 105 mm/year (July 30th, 1995 – December 11th, 1995) and 64 mm/year (December 11th, 1995 – February 9th, 1997) from two pairs of ERS satellite images (C-band, wavelength = 0.056 m) (Table 5). In this study, a subsidence rate of 476 mm/year has been measured from interferogram B, Figure 5.

Such a great increase can be understood from the following observations. In 2006, Shalev *et al.* [28] published the results of a sinkholes inventory constructed for the western side of the Dead Sea. They recorded sinkholes from inventory maps produced in 1980, 1990, 1997, 2001, 2003, and 2004. From their work, as well as from the one of Shirman and Rybakov [29] and from a communication provided by Eli Raz (Geological Survey of Israel), a curve with the cumulative number of sinkholes that have affected

the western shore between 1980 and 2009 had been produced (Fig. 12). A constant increase is noticeable from 1991 to 1999, followed by a drastic acceleration.

An increase in the gradient of the curve occurs around the year 2000, which represents an aggravation of the sinkhole hazard. This fact was also recorded along the Jordanian coast of the Dead Sea, either through the widening of cracks in the farming zone of Ghor al Haditha area – Southern Dead Sea [19], or throughout a number of major incidents as presented in the introduction.

During the period of observation of Baer *et al.* [14] -from July 30th, 1995 to February 9th, 1997- the number of sinkholes ranges from 156 to 212. During the period of observation with ALOS Palsar (November 15, 2007 – February 15, 2008), the number of sinkholes reached about 2500, i.e. ten times more. By comparison, the subsidence rate increased four times. Of course, subsidence and sinkholes are different in their origin but they are closely related phenomena. They appear frequently together along the Dead Sea shore. They are two types of vertical ground deformation with different dimensions and rates of development. The formation processes are different. Sinkholes are the consequences of a gradual or sudden collapse of the ground into a subsurface cavity while subsidence results from consolidation due to lowering of the water level and the decrease in intergranular pore water pressure.

The small number of measurements limits the interpretation but suggests that the present day rates of subsidence could be higher than the ones measured more than ten years ago. Repeated field surveys in Ghor Al Haditha have clearly showed a drastic increase in the development of sinkholes and subsidence. New places have been affected, generally seawards.

5. Conclusions

From five interferograms spanning from November 15, 2007 to May 17, 2008, three areas affected by ground subsidence have been detected. The one illustrated in Figure 5, zone "A", shows that deformation was already active before the earthquakes of April 13, 2008 and increased drastically during the whole period of monitoring. The period of maximum deformations (April 1, 2008 to May 17, 2008) is contemporaneous to the earthquakes. However, to make a possible correlation with seismic activity that would increase the number of collapses; a precise location of the epicenter together with a precise dating of sinkhole occurrences is needed. The lack of accuracy impedes the establishment of a robust correlation between karst development and seismic events. Therefore, the deformations could be related to dissolution of shallow salt levels along ancient tectonic lineaments rather than faulting.

The geometric characteristics of the deformation field in zone "A" are relevant for understanding the ongoing problems that affect saltpan 18. It is worth mentioning here that

the failure of saltpan 18 would result in the sudden release of 90 million cubic meters of brine in the Dead Sea with effects difficult to assess at the western coast.

High rates of subsidence have been measured in the northern Lynch Strait. These data indicate that the subsidence phenomena follow the same increasing trend as the formation of sinkholes. More measurements should be carried out in order to refine this observation.

Finally, the emersion of the Lynch Strait some thirty years ago most likely lead to the development of a new salt karst. The energy available for the evolution of the system derives from the Dead Sea (base) level lowering and from the active tectonic setting as shown here. Its development is conditioned by the supply of underground unsaturated water coming from the western side, the Lisan area, and from the flood channel which evacuates the water coming from Wadi Hasa, Wadi Numeira, and Wadi Araba.

References

- [1] Hall J.K., Dead Sea geophysical survey - bathymetric chart, Geological Survey of Israel, Marine Geology Division, Jerusalem, 1979.
- [2] Topographic maps edited by the Soviet government: Sovetskaiia Armiia, Generalnyi shtab. Sheet 8-36-35 at 100k scale, survey 1980, and sheet 8-36-35-2 at 50k scale, survey 1993.
- [3] Images courtesy of Earth Sciences and Image Analysis Laboratory, NASA Johnson Space Centre. Mission: STS099, Roll: 751, Frame: 24.
- [4] Knill J., Report on a Visit 8-11 January 1993 Extension West of Lisan Peninsula Sinkholes Along Access Road, The Arab Potash project, Amman, unpublished report, 1993, 19 p.
- [5] Itanar A., Reizman Y., Air Photo Survey of Sinkholes in the Dead Sea Area, Geological Survey of Israel - Current Research 12 (2000) 21-24.
- [6] Shamir, G., The active structure of the Dead Sea Depression, in: Enzel, Y., Agnon, A., Stein, M. (Eds.), *New Frontiers in Dead Sea Paleoenvironmental Research*, Geological Society of America Special Papers 401, 2006, pp. 15-32.
- [7] Closson D., LaMoreaux P.E., Abou Karaki N., al-Fugha H., Karst system developed in salt layers of the Lisan Peninsula, Dead Sea, Jordan, *Environmental Geology* 52, 1 (2007) 155-172.
- [8] Gabriel A.K., Goldstein R.M., Zebker H.A., Mapping small elevation changes over large areas: differential radar interferometry, *J. Geophys. Res.* 94 (B7) (1989) 9183-9191.
- [9] Zebker H.A., Rosen P., Goldstein R.M., Gabriel A., Werner C., On the derivation of coseismic displacement fields using differential radar interferometry: the Landers earthquake, *J. Geophys. Res.* (1995).
- [10] Riedmann M., Haynes M., Developments in synthetic aperture radar interferometry for monitoring geohazards, Geological Society, London, Special Publications, 283 (2007) 45-51.
- [11] Cornet Y., Doulliez J.-Y., Moxhet J., Closson D., Kourgli A., Ozer A., Use of ERS Tandem Data to Produce Digital Elevation Models by Interferometry and Study Land Movements by Differential Interferometry in Calabria and Jordan, 3rd ERS Symposium, Florence, March 14–21, Italy (1997) <http://earth.esa.int/symposia/papers/ozel/>
- [12] Derauw D., Moxhet J., Multiple Image SAR Interferometry, Fringe'96, ESA Workshop on Applications of ERS SAR Interferometry, Remote Sensing Laboratories, University of Zurich, September 30 - October 2, Switzerland (1996) <http://www.geo.unizh.ch/rsl/fringe96/papers/deraaw/>
- [13] Derauw D., Phasimétrie radar à synthèse d'ouverture: théorie et applications, Université de Liège Belgium, 1999, 118 p.
- [14] Baer G., Schattner U., Wachs D., Sandwell D., Wdowski S., Frydman S., The Lowest Place on Earth is Subsiding - An InSAR (Interferometric Synthetic Aperture Radar) Perspective, *Geological Society of America Bulletin* 114, 1 (2002) 12-23.
- [15] Shimoni M., Hanssen R.F., Van Der Meer F., Kampes B.M., Ben Dor E., Salt Diapir Movements Using SAR Interferometry in the Lisan Peninsula, Dead Sea Rift, *Proceedings of SPIE* 4543 (2002) 151-160.
- [16] Closson D., Abou Karaki N., Hansen H., Derauw D., Barbier C., Ozer A., Space-borne Radar Interferometric Mapping of Precursory Deformations of a Dyke Collapse - Dead Sea Area - Jordan, *International Journal of Remote Sensing* 24, 4 (2003) 843-849.
- [17] Abelson M., Baer G., Shtivelman V., Wachs D., Raz E., Crouvi O., Kurzo, I., Yechieli Y., Collapse-Sinkholes and Radar Interferometry Reveal Neotectonics Concealed Within the Dead Sea, *Geophysical Research Letters* 30, 10, 1545 (2003) 521–52/4.
- [18] Wei M., Sandwell D., Decorrelation of ALOS and ERS Interferometry Over Vegetated Areas in California, 3rd ALOS PI Symposium Proceedings, Kona, Hawaii, (2009) 9th - 13th November.
- [19] Nitti D.O., De Vitis L., Nutricato R., Bovenga F., Refice A., Wasowski J., Multi-temporal L-band SAR interferometry confirms

Acknowledgements

The research of Damien Closson, Nada Milisavljević, Frédéric Hallot, and Marc Acheroy is supported by the Royal Military Academy of Belgium. Part of the work of Najib Abou Karaki was done in the framework of the EC supported project APAME ICA3-CT 2002-10024. The support of both parties is highly appreciated.

Particular thanks to the Deanship of Scientific Research of the University of Jordan for the coordination of the field work. We also thank all who have accompanied us on the ground, especially Mr Azzam Azara, Nael Abbadi, Ashraf Shhadat, Majida Farraj, and Mahmoud Obeidat.

We thank C. Castañeda, F. Gutierrez and M. Meghraoui for the time they spent to read carefully the first version of the text and improve our work through constructive remarks, observations and comments.

- C-band spatial patterns of subsidence in the ancient Wieliczka Salt Mine (UNESCO Heritage Site, Poland), *Advances in the Science and Applications of SAR Interferometry*, ESA ESRIN, Frascati, Italy (2009) 30th November - 4th December.
- [20] Closson D., Structural Control of Sinkholes and Subsidence Hazards along the Jordanian Dead Sea Coast, *Environmental Geology* 47, 2 (2005) 290-301.
- [21] Closson D., Abou Karaki N., Salt karst and tectonics: sinkholes development along tension cracks between parallel strike-slip faults, Dead Sea, Jordan, *Earth Surface Processes and Landforms* 34, 10 (2009) 1408-1421.
- [22] Arieh E., Rotstein Y., Peled U., The Dead Sea earthquake of April 1979, *Bulletin of the Seismological Society of America* 72 (1982) 1627-1634.
- [23] Closson D., Abou Karaki N., Human-induced geological hazards along the Dead Sea coast, *Environmental Geology* 58, 2 (2009) 371-380.
- [24] Salameh E., El-Naser H., Changes in the Dead Sea Level and their Impacts on the Surrounding Groundwater Bodies, *Acta Hydrochemica et Hydrobiologica* 28 (2000) 2-33.
- [25] Salameh E., El-Naser H., The Interface Configuration of the Fresh / Dead Sea Water – Theory and Measurements, *Acta Hydrochemica et Hydrobiologica* 28, 6 (2000) 323-328.
- [26] Yechieli Y., Kafri U., Goldman M., Voss C., Factors Controlling the Fresh-Saline Interface Configuration in the Dead Sea Coastal Aquifers: Synthesis of TDEM Surveys and Numerical Ground-Water Modeling, *Hydrogeology Journal* 9 (2000) 367-377.
- [27] <http://earthquake.usgs.gov/eqcenter/shakemap/atlas/shake/197904231301/>
- [28] Shalev E., Lyakhovskiy V., Yechieli Y., Salt dissolution and sinkhole formation along the Dead Sea shore, *Journal of Geophysical Research* 111 (2006) B03102, doi:10.1029/2005JB004038
- [29] Shirman B., Rybakov M., Sinkholes along the Dead Sea Coast and Their Development, FIG Working Week 2009. Surveyors Key Role in Accelerated Development, May 3-8, Eilat, Israel (2009) <http://www.fig.net/pub/fig2009/papers/ts04e/>